Published in final edited form as:
Science. 2011 April 8; 332(6026): 234–238. doi:10.1126/science.1198542.

A dynamic knockout reveals that conformational fluctuations influence the chemical step of enzyme catalysis

Gira Bhabha[1], **Jeeyeon Lee**[2,‡], **Damian C. Ekiert**[1], **Jongsik Gam**[2], **Ian A. Wilson**[1], **H. Jane Dyson**[1], **Stephen J. Benkovic**[2], and **Peter E. Wright**[1,*]

[1]Department of Molecular Biology and Skaggs Institute for Chemical Biology, The Scripps Research Institute, La Jolla, California 92037

[2]Department of Chemistry, Pennsylvania State University, University Park, Pennsylvania

Abstract

Conformational dynamics play a key role in enzyme catalysis. While protein motions have clear implications for ligand flux, a role for dynamics in the chemical step of enzyme catalysis has not been clearly established. We generated a mutant of *E. coli* dihydrofolate reductase (DHFR) that abrogates millisecond time scale fluctuations in the enzyme active site without perturbing its structural and electrostatic preorganization. Remarkably, this dynamic knockout severely impairs hydride transfer. Thus we have found a link between conformational fluctuations on the millisecond timescale and the chemical step of an enzymatic reaction, with broad implications for our understanding of enzyme mechanisms and for attempts to design novel protein catalysts.

Protein motions are critical for biological functions, but their precise role in enzyme catalysis remains unclear (1, 2). While there is convincing evidence that conformational fluctuations are essential for mediating substrate and cofactor binding as well as product release, and can be rate limiting for enzyme turnover (3–6), the importance of protein flexibility for progression along the chemical reaction coordinate remains a matter of debate (7, 8). In one view, electrostatic preorganization of the active site is considered to account fully for enzyme catalysis (9); on the other hand, hydrogen tunneling experiments suggest that a static model is inadequate and that fluctuations that reorganize the active site are required for the chemical step (7, 10, 11), which involves conformational sampling to facilitate hydrogen transfer as well as the transfer itself.

E. coli dihydrofolate reductase (*ec*DHFR) is a paradigm for understanding the relationship between structure, dynamics, and catalysis (4, 12–14). DHFR catalyzes the stereospecific reduction of dihydrofolate (DHF) to tetrahydrofolate (THF), using reduced nicotinamide adenine dinucleotide phosphate (NADPH) as cofactor. Five intermediates have been identified in the steady state catalytic cycle (7): E:NADPH, E:NADPH:DHF, E:$NADP^+$:THF, E:THF, and E:NADPH:THF (Fig. 1). Large conformational changes are observed in the Met20 loop (residues 9–24) between the Michaelis complex E:NADPH:DHF (modeled by E:$NADP^+$:folate (FOL) for structural studies) and the product complex, E:$NADP^+$:THF (13). The Met20 loop adopts two dominant conformations: the ‘closed’ conformation, in which the loop packs tightly against the nicotinamide ring of the cofactor, and the ‘occluded’ conformation, in which the loop projects into the active site and sterically blocks the nicotinamide binding pocket. The holoenzyme (E:NADPH) and the model Michaelis complex (E:$NADP^+$:FOL) are in the ‘closed’ conformation, while the three

*To whom correspondence should be addressed. wright@scripps.edu.
‡Current address: College of Pharmacy, Ajou University, San 5, Woncheon-dong, Yeongtong-Gu, Suwon, Korea 443-749

product complexes (E:$NADP^+$:THF, E:THF, E:NADPH:THF) adopt the 'occluded' conformation (Fig. 1), which is stabilized by hydrogen bonds between Asn 23 and the backbone and side chain of Ser 148 (13, 15).

In crystal structures of human and other vertebrate DHFRs, the Met20 loop is invariably closed (16). Alignment of the human and *E. coli* DHFR protein sequences suggests that the occluded conformation is destabilized in the human enzyme due to an inability to form the stabilizing hydrogen bond made by the S148 side chain in *ec*DHFR (Fig. S1). In addition, a polyproline sequence (PWPP) at the end of the 'Met20' loop of human DHFR may render the loop less flexible than in the *E. coli* enzyme. We hypothesized that a "dynamic knockout" mutant designed to impair the dynamics of the Met20 loop in *ec*DHFR would give direct information on the role of active-site loop fluctuations in catalysis by the *E. coli* enzyme. To this end, the *ec*DHFR mutant N23PP/S148A (Fig. 1) was engineered and characterized using X-ray crystallography, NMR spectroscopy and kinetic analysis (17).

To assess the effect of the mutations on *ec*DHFR activity, we carried out both steady state and pre-steady state kinetic measurements on N23PP/S148A DHFR. The overall turnover rate (k_{cat}) is significantly lower than for the wild type enzyme (Table 1). For wild type *ec*DHFR, k_{cat} is determined by dissociation of the THF product from the E:NADPH:THF complex (Fig.1) (10), whereas for the mutant enzyme, the magnitude of k_{cat} is determined by dissociation of the $NADP^+$ cofactor (Fig. S2). Thus, the reduced flexibility inherent in the design of N23PP/S148A *ec*DHFR imposes a change in the kinetic step that determines the steady state k_{cat}. The hydride transfer step was monitored directly in pre-steady state kinetic experiments as described in supporting online material (Fig. S3). Remarkably, the rate of hydride transfer at pH 7.0 is 14 s^{-1} for the N23PP/S148A DHFR mutant, which is significantly slower than for wild-type *ec*DHFR (Table 1) (18). The measured rate for the chemical step has a primary kinetic isotope effect (KIE) of 3.0 (the same as the wild-type enzyme), consistent with the difference in zero point energies between the two hydrogen isotopes and confirming that we are, indeed, directly observing the rate of hydride transfer.

Structural differences between N23PP/S148A *ec*DHFR and wild-type *ec*DHFR were assessed by determining the crystal structure of the mutant enzyme in complex with $NADP^+$ and folate and comparing it to the wild-type E:$NADP^+$:FOL complex (13). To eliminate differences in refinement methods, the wild-type E:$NADP^+$:FOL complex (13) was re-refined using the structure factors deposited in the PDB (code:1RX2), as described in supporting online material. The re-refined structure shows only very minor differences from the original 1RX2 coordinates. The N23PP/S148A *ec*DHFR at 1.6 Å resolution is almost identical to 1RX2-re-refined at 1.8 Å (13) (Fig. 2). Some minor adjustments at the end of the Met20 loop are observed, due to the proline insertion, but the loop is clearly in the closed conformation as in the wild-type E:$NADP^+$:FOL complex. The ligand (Fig. S4) and active-site side chain conformations are maintained (Fig. 2), as are the hydrogen bonds (Table S2) and the locations of water molecules in the active site. The distance between hydride donor and acceptor atoms is slightly decreased (from 3.3 Å to 2.9 Å) in the N23PP/S148A mutant. This decrease cannot account for the impaired hydride transfer rate in the mutant, as a shorter distance would be expected to facilitate hydride transfer, not inhibit it. The similarity of the backbone conformations of the wild-type and N23PP/S148A E:$NADP^+$:FOL complexes in solution is also illustrated by the near identity of ^{15}N and ^{1}H chemical shifts (Fig. S5).

The conservation of side chain conformations and water molecules in the active site of the wild type and mutant enzymes argues for a very similar electrostatic environment. However, a slight change in the Met20 side chain required further investigation. It has been proposed that the Met20 S_δ atom might assist catalysis by increasing the pK_a of the substrate, thereby

promoting protonation of the N5 atom of the pterin (19). The Met20 S_δ atom in N23PP/S148A E:$NADP^+$:FOL is shifted ~0.3 Å relative to its position in the wild-type complex (20) (Fig. S6). We measured the pH-dependence of hydride transfer in the N23PP/S148A mutant to ensure that the apparent small difference in the position of the Met20 S_δ atom does not impair hydride transfer by decreasing the pK_a for N5. The hydride transfer rate for N23PP/S148A ecDHFR decreases with increasing pH (21) with a pK_a of 6.7 ± 0.1, which is the same, within experimental error, as the value for the wild-type enzyme (6.5 ± 0.1). If anything, the pK_a is slightly higher for the mutant enzyme, which would facilitate hydride transfer rather than inhibit it. Thus, the X-ray and NMR data and the pK_a measurements show that there are no significant differences in the structure or electrostatic environment of the active site between the E:$NADP^+$:FOL complexes of wild-type and N23PP/S148A ecDHFR.

In wild-type ecDHFR, the Met20 loop adopts the closed ground state conformation in the Michaelis model complex, E:$NADP^+$:FOL, and the occluded ground state conformation in the product ternary complex, E:$NADP^+$:THF (13, 15, 22). Previous NMR studies identified marker resonances, mostly in the Met20 and FG loops, for which ^{15}N and ^1H chemical shifts differ significantly between the closed and occluded conformations (22). Unlike the wild-type enzyme, the E:$NADP^+$:FOL and E:$NADP^+$:THF complexes of the N23PP/S148A mutant enzyme have almost identical ^1H and ^{15}N chemical shifts for most residues, including those in the Met20, FG, and GH loops (Fig. 3 and Fig. S7), showing that the mutant enzyme remains in the closed conformation across the chemical step. The occluded conformation itself is not relevant to hydride transfer, which takes place within an ensemble of states in which the active site loops are closed (13). However, the fact that the mutant enzyme is unable to adopt an occluded conformation suggested that the flexibility of the active site loops may be significantly dampened and prompted us to examine the dynamics of the N23PP/S148A Michaelis model complex (E:$NADP^+$:FOL)..

Carr-Purcell-Meiboom-Gill (CPMG)-based R_2 relaxation dispersion NMR experiments were used to monitor the sampling of higher energy, lowly populated conformational substates that are associated with millisecond timescale structural fluctuations (23, 24). Previous studies of wild-type *ec*DHFR revealed millisecond timescale motions in the active site and C-terminal region in all five intermediate complexes of the catalytic cycle (4, 25). Surprisingly, relaxation dispersion experiments on the E:$NADP^+$:FOL complex of N23PP/S148A DHFR showed no dispersion for any active site residues (with the sole exception of Ala 9), indicating that fluctuations on the millisecond timescale are abrogated in the mutant enzyme complex (Fig. 4). Residues associated with the C-terminus, however, undergo fluctuations on the millisecond timescale similar to those in the wild-type enzyme, confirming that the mutations affect dynamics only in the active site. R_1, R_2 and heteronuclear NOE experiments show that the Met20 loop of N23PP/S148A in the E:$NADP^+$:FOL complex is rather rigid on the picosecond to nanosecond timescale, as in the wild-type enzyme (26) (Fig. S8). Several residues exhibiting exchange contributions from millisecond timescale conformational fluctuations in the active site loops have elevated R_2 values in wild-type *ec*DHFR, while the values for these residues remain close to average for the N23PP/S148A mutant, suggesting that the mutations have not simply moved the motions to a faster, microsecond timescale. No minor resonances, which might be expected if there was a small population (~3% or higher) of an alternative Met20 loop conformation in slow exchange with the closed ground state, are observed in the ^{15}N-HSQC spectrum of N23PP/S148A E:$NADP^+$:FOL. Thus, we conclude that the millisecond time scale fluctuations in active site of the wild-type enzyme have been abolished in the N23PP/S148A mutant.

To obtain further insights into the effects of the N23PP/S148A mutations, we generated two additional *ec*DHFR mutants, N23PP and S148A. The N23PP mutation is, in itself, sufficient

to abrogate the active-site flexibility required for efficient catalysis. The hydride transfer rate for the N23PP mutant ($14 \pm 1\ s^{-1}$) is the same as for N23PP/S148A, while NMR experiments show that the Met20 loop remains in the closed conformation across the hydride transfer step, and that the millisecond time scale fluctuations in the active site are quenched in the E:$NADP^+$:FOL complex of N23PP DHFR (Table 1, Fig. 4, Fig.S9). An analysis of S148A *ec*DHFR reveals that the decreased hydride transfer rate does not simply arise from impairment of the closed to occluded transition in the mutant enzymes. S148A *ec*DHFR also remains in the closed ground state conformation across the hydride transfer step (Fig. S10), yet its hydride transfer rate ($157\ s^{-1}$) is decreased only slightly from that of the wild-type enzyme (27). R_2 dispersion experiments on the S148A E:$NADP^+$:FOL complex show that, while the millisecond timescale dynamics are dampened compared to wild-type, several active-site residues do retain flexibility, sampling higher energy conformational substates that do not correspond to the occluded state (Fig. 4 and Fig. S11). We conclude that, unlike the N23PP and N23PP/S148A mutants, the S148A mutant retains residual motions in the active site, which are not associated with the closed-occluded transition, but which likely play a role in promoting hydride transfer.

Considering that the E:$NADP^+$:FOL complexes, which are models for the Michaelis complex, have virtually identical active site structures in both the N23PP/S148A mutant and wild-type enzyme, it is most unlikely that hydride transfer is impaired in the mutant because of differences in the structural and electrostatic environment of the active site. While the ground state structures are almost indistinguishable, the wild-type and mutant enzymes differ substantially in their ability to sample alternative ground state active site conformations and access higher energy conformational substates through millisecond time scale fluctuations. The ground state conformational change between the closed Michaelis complex and the occluded product complex in wild-type *ec*DHFR is not observed for any of the three mutants, since the active site loops are restrained in the closed conformation. The millisecond timescale motions in the active site that allow the wild-type enzyme to sample higher energy substates are eliminated in the N23PP/S148A and N32PP mutants, while the S148A mutant still retains some flexibility, and has a correspondingly higher rate of hydride transfer. We, therefore, conclude that the significantly decreased rate of hydride transfer in the N23PP/S148A and N32PP mutant enzymes does not result from changes in structural or electrostatic preorganization of the active site, but from impaired flexibility.

Molecular simulations consistently show that Met20 loop residues move closer to the cofactor on progressing from reactant to transition state. These residues are predicted to play an important role in electrostatic stabilization of the transition state and in promoting protonation of the N5 atom of the pterin moiety of the substrate (19, 28, 29). This movement is likely required to tightly close and compact the active site, to correctly orient and constrain the substrate and cofactor, and to promote hydride transfer by reducing the distance between the donor and acceptor atoms. Although the active site of the N23PP/S148A mutant is fully preorganized in the ground state, millisecond timescale fluctuations of the active site are restricted such that the enzyme cannot efficiently sample higher energy conformational substates that are conducive to formation of the transition state; impairment of conformational fluctuations in the active site leads to strong inhibition of the chemical step. Fine-tuning of conformational flexibility is likely a general phenomenon that can be harnessed in engineering of efficient protein catalysts.

Supplementary Material

Refer to Web version on PubMed Central for supplementary material.

References and Notes

1. Hammes-Schiffer S, Benkovic SJ. Annu. Rev. Biochem. 2006; 75:519. [PubMed: 16756501]
2. Henzler-Wildman K, Kern D. Nature. 2007; 450:964. [PubMed: 18075575]
3. Wolf-Watz M, et al. Nat Struct Mol Biol. 2004; 11:945. [PubMed: 15334070]
4. Boehr DD, McElheny D, Dyson HJ, Wright PE. Science. 2006; 313:1638. [PubMed: 16973882]
5. Doucet N, Watt ED, Loria JP. Biochemistry. 2009; 48:7160. [PubMed: 19588901]
6. Watt ED, Shimada H, Kovrigin EL, Loria JP. Proc. Natl. Acad. Sci. U. S. A. 2007; 104:11981. [PubMed: 17615241]
7. Nagel ZD, Klinman JP. Nat Chem Biol. 2009; 5:543. [PubMed: 19620995]
8. Kamerlin SC, Warshel A. Proteins. 2010; 78:1339. [PubMed: 20099310]
9. Pisliakov AV, Cao J, Kamerlin SC, Warshel A. Proc. Natl. Acad. Sci. U. S. A. 2009; 106:17359. [PubMed: 19805169]
10. Liang ZX, Lee T, Resing KA, Ahn NG, Klinman JP. Proc. Natl. Acad. Sci. U. S. A. 2004; 101:9556. [PubMed: 15210941]
11. Benkovic SJ, Hammes-Schiffer S. Science. 2003; 301:1196. [PubMed: 12947189]
12. Fierke CA, Johnson KA, Benkovic SJ. Biochemistry. 1987; 26:4085. [PubMed: 3307916]
13. Sawaya MR, Kraut J. Biochemistry. 1997; 36:586. [PubMed: 9012674]
14. Schnell JR, Dyson HJ, Wright PE. Annu. Rev. Biophys. Biomol. Struct. 2004; 33:119. [PubMed: 15139807]
15. Venkitakrishnan RP, et al. Biochemistry. 2004; 43:16046. [PubMed: 15609999]
16. Davies JF 2nd, et al. Biochemistry. 1990; 29:9467. [PubMed: 2248959]
17. Materials and methods are available as supporting material on *Science* Online
18. Cameron CE, Benkovic SJ. Biochemistry. 1997; 36:15792. [PubMed: 9398309]
19. Khavrutskii IV, Price DJ, Lee J, Brooks CL 3rd. Protein Sci. 2007; 16:1087. [PubMed: 17473015]
20. The terminal methyl of M20 is not clearly defined by the electron density in 1RX2 and in 1RX2-rerefined, and is likely flexible. In addition, density for water 47 is observed in 1RX2-rerefined, but was not built into 1RX2. A discussion on building M20 and water47 into 1RX2-rerefined is included in the Supporting Online Material.
21. At basic pHs, the hydride transfer rate (k_{hyd}) is decreased to 3.3 s-1 for N23PP/S148A due to the limited sources of protons for the hydride transfer step. The pKa values are derived from fitting the pH Vs. k_{hyd} profile as described in the supplementary material
22. Osborne MJ, Venkitakrishnan RP, Dyson HJ, Wright PE. Protein Sci. 2003; 12:2230. [PubMed: 14500880]
23. Palmer AG 3rd, Kroenke CD, Loria JP. Methods Enzymol. 2001; 339:204. [PubMed: 11462813]
24. Mittermaier A, Kay LE. Science. 2006; 312:224. [PubMed: 16614210]
25. McElheny D, Schnell JR, Lansing JC, Dyson HJ, Wright PE. Proc. Natl. Acad. Sci. U. S. A. 2005; 102:5032. [PubMed: 15795383]
26. Osborne MJ, Schnell J, Benkovic SJ, Dyson HJ, Wright PE. Biochemistry. 2001; 40:9846. [PubMed: 11502178]
27. Miller GP, Wahnon DC, Benkovic SJ. Biochemistry. 2001; 40:867. [PubMed: 11170407]
28. Agarwal PK, Billeter SR, Rajagopalan PT, Benkovic SJ, Hammes-Schiffer S. Proc. Natl. Acad. Sci. U. S. A. 2002; 99:2794. [PubMed: 11867722]
29. Garcia-Viloca M, Truhlar DG, Gao J. Biochemistry. 2003; 42:13558. [PubMed: 14622003]

30. The authors acknowledge L. Tuttle for invaluable discussions, S. Bae for NMR data on the S148A mutant, H. Tien and D. Marciano of the Robotics Core at the Joint Center for Structural Genomics (JCSG) for automated crystal screening, and X. Dai for technical assistance with crystallographic data collection. This work was supported by the National Institutes of Health Grant GM75995 and the Skaggs Institute of Chemical Biology. The JCSG is supported by NIH National Institute of General Medical Sciences (NIGMS) (U54 GM094586). DCE is supported by a predoctoral fellowship from the Achievement Rewards for College Scientists Foundation, and Grant GM080209 from the NIH Molecular Evolution Training Program. The GM/CA CAT 23-ID-D has

been funded in whole or in part with federal funds from National Cancer Institute (Y1-CO-1020) and NIGMS (Y1-GM-1104). Use of the Advanced Photon Source (APS) was supported by the U.S. Department of Energy, Basic Energy Sciences, Office of Science, under contract no. DE-AC02-06CH11357. The content is solely the responsibility of the authors and does not necessarily represent the official views of NIGMS or the NIH. Coordinates and structure factors of N23PP/S148A ecDHFR and 1RX2-re-refined are deposited in the Protein Data Bank (PDB code 3QL0 and 3QL3). Author contributions: GB and PEW designed the research. GB performed NMR experiments. GB and DCE performed crystallography experiments and structure refinement. IAW supervised structure refinement. JL and JG performed kinetic experiments and analysis. GB, PEW and SJB analysed and interpreted the data. GB, PEW and JL wrote the manuscript. IAW, HJD and SJB edited the manuscript.

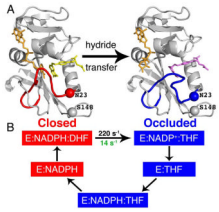

Fig. 1.

Conformational changes that occur during the *E. coli* DHFR catalytic cycle. (**A**) Left, cartoon representation of E:$NADP^+$:FOL crystal structure (1RX2, model for the Michaelis complex, E:NADPH:DHF) in the closed conformation. Right, crystal structure of E:$NADP^+$:ddTHF (1RX4, model for the product complex) in the occluded conformation. $NADP^+$ is shown in orange; FOL is shown in yellow and ddTHF in magenta. Red, Met20 loop in the closed conformation; blue, Met20 loop in the occluded conformation. The sites of mutation, N23 and S148 are shown as spheres. (**B**) Intermediates in the wild type *E. coli* DHFR catalytic cycle. Intermediates shown in red are in the closed conformation, and those in blue are in the occluded conformation. Prior to hydride transfer the Met20 loop is in the closed conformation, where it packs tightly against the nicotinamide ring of $NADP^+$. Following hydride transfer, the Met20 loop adopts the occluded conformation, in which the nicotinamide ring of $NADP^+$ is sterically hindered from binding in the active site. $NADP^+$ undergoes a concurrent conformational change in which the nicotinamide ring is expelled from the binding pocket, initiating $NADP^+$ release from the ternary product complex. The rate of hydride transfer in the wild type and N23PP/S148A mutant enzyme is indicated in black and green, respectively. Note that the mutation alters the pathway utilized for product and $NADP^+$ release, as shown in Fig. S2.

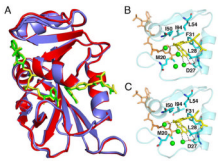

Fig. 2.

The three-dimensional structures of the E:$NADP^+$:FOL complexes of the N23PP/S148A mutant and wild-type *E. coli* DHFR are almost identical. (**A**) Superposition of the crystal structures of wild-type *E. coli* DHFR (1RX2) and N23PP/S148A *E. coli* DHFR. Wild-type *E. coli* DHFR is shown in red, with yellow ligands and N23PP/S148A *E. coli* DHFR is shown in purple, with green ligands. (**B**) Active site configuration for wild-type ecDHFR (1RX2-re-refined). Folate is colored yellow, $NADP^+$ orange, the waters are shown as green spheres, and key active-site residues are in blue sticks. (**C**) Active site configuration for N23PP/S148A ecDHFR. Colors are the same as for **B.** For clarity, only the major conformation of the glutamate moiety of folate is shown. The active site configurations are almost identical for wild type and N23PP/S148A ecDHFR, including placement of polar residues, key hydrophobic residues and waters, showing that the electrostatic nature of the active site is unchanged by the mutations.

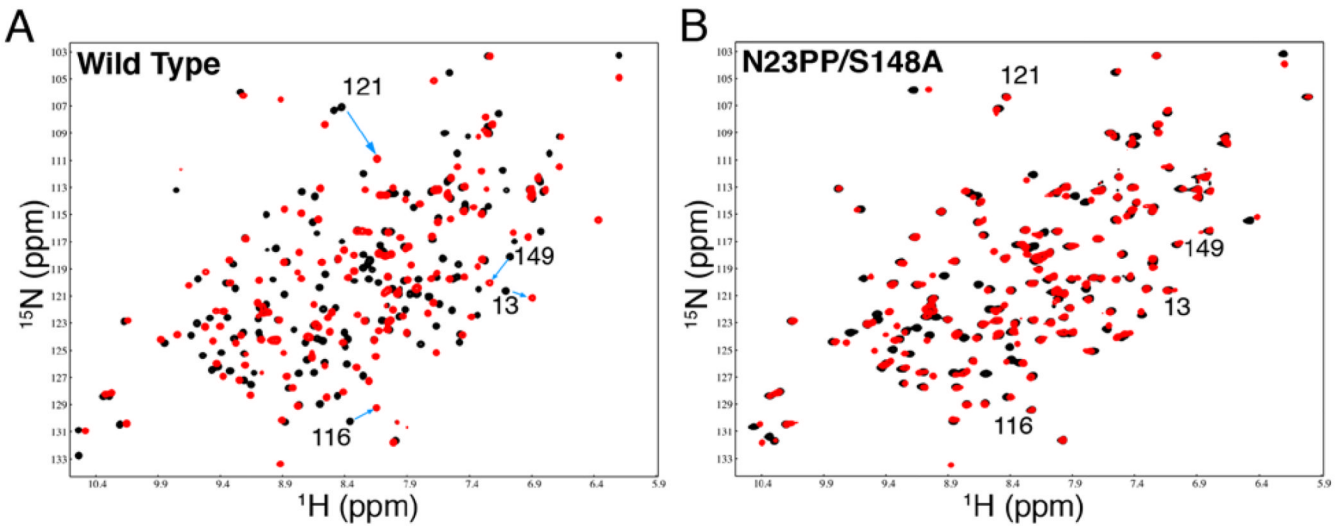

Fig. 3.

The Met20 loop of N23PP/S148A *E. coli* DHFR remains in the closed position across the chemical step. (**A**) ^{1}H-^{15}N HSQC spectra of wild-type E:NADP^{+}:FOL (model Michaelis complex, black) in the closed conformation and E:NADP^{+}:THF (product complex, red) in the occluded conformation. Large chemical shift differences are observed, particularly for residues in regions that undergo the closed-to-occluded structural change. Chemical shift changes from closed (black) to occluded (red) are indicated by arrows for several residues in the active site loops. (**B**) ^{1}H-^{15}N HSQC spectra of N23PP/S148A E:NADP^{+}:FOL (model Michaelis complex, black) and E:NADP^{+}:THF (product complex, red). The ^{1}H-^{15}N HSQC spectra for the complexes of the mutant enzyme are similar; the cross peaks corresponding to the active site loops do not shift, and appear in the position corresponding to the closed conformation for both complexes. A quantitative chemical shift analysis is presented in Fig. S8.

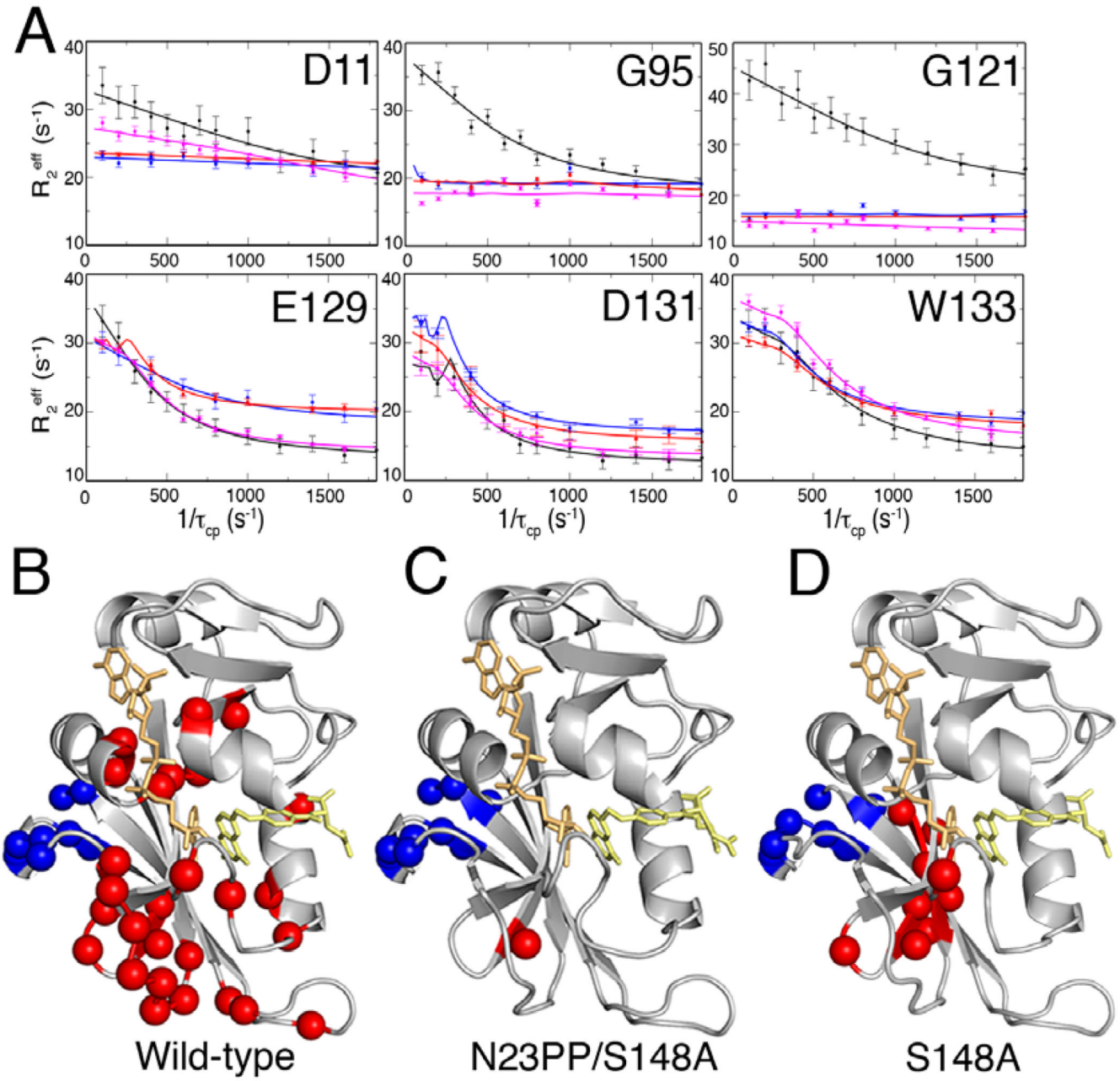

Fig. 4.

Millisecond timescale dynamics in the active site loops of the E:$NADP^+$:FOL complex are impaired by the N23PP/S148A mutation. (**A**) Representative ^{15}N R_2 relaxation dispersion curves for wild type (black), N23PP/S148A (red), N23PP (blue) and S148A (magenta) E:$NADP^+$:FOL. Dispersion data were collected at pH 7.6 and at 301 K. Top, active site loop residues (11, 95, 121), for which the dispersion observed in wild type E:$NADP^+$:FOL is not observed in either N23PP/S148A or N23PP E:$NADP^+$:FOL. S148A retains dispersion for residue 11 and other active site residues, shown in Fig. S11. Bottom, C-terminal associated residues (129, 131, 133), for which dispersion is observed for the wild type and mutant proteins. Residues which display ^{15}N relaxation dispersion in the E:$NADP^+$:FOL complex are mapped onto the structure for wild type (**B**), N23PP/S148A (**C**) and S148A (**D**). 1RX2

coordinates are used for representations in **B** and **D**. Red spheres indicate active site-associated residues for which R_2 dispersion is observed. Blue spheres indicate C-terminal-associated residues for which R_2 dispersion is observed. $NADP^+$ is shown as orange sticks, FOL as yellow sticks. For clarity, only the major conformation of the glutamate moiety of folate is shown.

Table 1

Kinetic parameters

	Wild type [a]	**N23PP-S148A**	**N23PP**	**S148A**[b]
k_{cat} (s^{-1})	12	1.8 ± 0.6	2.5 ± 1	6.6 ± 0.8
k_{hyd} (s^{-1})	220 ± 10	13.9 ± 0.6	14.2 ± 1	157 ± 3
pK_a	6.5 ± 0.1	6.7 ± 0.1	6.6 ± 0.1	ND[c]
KIE (k_{hyd})	3.0 ± 0.1	3.0 ± 0.1	ND[c]	2.7 ± 0.1

[a] Kinetic parameters for wild type enzyme as reported in ref. 11

[b] Kinetic parameters for the S148A mutant as reported in ref. 26

[c] ND, not determined